Further Observations Of A Decreasing Atmospheric Co2 Uptake Capacity In The Canada Basin (Arctic Ocean) Due To Sea Ice Loss

B. G. T. Else, R. J. Galley, B. Lansard, D. G. Barber, K. Brown, L. A. Miller, A. Mucci, T. N. Papakyriakou, J. E. Tremblay, S. Rysgaard

Sea ice loss and the changing atmospheric CO_2 uptake capacity of the Arctic Ocean: Insights from the southeastern Canada Basin

Brent G.T. Else, R.J. Galley, B. Lansard, D.G. Barber, K. Brown, L.A. Miller, A. Mucci, T.N. Papakyriakou, J.-É. Tremblay, S. Rysgaard

Abstract

Using data collected in 2009, we evaluated the potential for the southeastern Canada Basin (Arctic Ocean) to act as an atmospheric CO_2 sink under the summertime ice-free conditions expected in the near future. Beneath a heavily decayed ice cover, we found surprisingly high pCO_{2sw} (~290-320 μatm), considering that surface water temperatures were low and the influence of ice melt was strong. A simple model simulating melt of the remaining ice and exposure of the surface water for 100 days revealed a weak capacity for atmospheric CO_2 uptake (mean flux: -2.4 mmol m^{-2} d^{-1}), due largely to warming of the shallow mixed layer. Our model result is 60% lower than estimates derived during the previous summer in the ice-free southwestern Canada Basin. The discrepancy is likely caused to some degree by regional variability, but may also reflect increased ventilation of the surface mixed layer due to sea ice loss.

1. Introduction

One outcome of the recent retreat of Arctic sea ice is an increased potential for air-sea gas exchange. This phenomenon is particularly significant on the extensive Arctic shelves, where pronounced decreases in summer ice extent have progressively exposed the surface ocean over greater temporal and spatial scales (e.g. *AMAP,* 2011). Since the surface water of most Arctic shelf seas experience persistently low CO_2 partial pressures (pCO_{2sw}) during the open water season, the uptake of atmospheric CO_2 in these areas is thought to have increased as a result of sea ice loss (e.g. *Bates and Mathis*, 2009).

In light of this increased CO_2 uptake capacity on the shelves, there has been an emerging debate about the potential for the deep Arctic basins to absorb more CO_2 as they become seasonally ice free (*Bates et al.,* 2006; *Cai et al.,* 2010; *Jutterström and Anderson,* 2010). The southwest portion of the Canada Basin (adjacent to the Chukchi Sea) has already experienced a significant northward migration of the summer ice edge (*Hutchings and Rigor,* 2012), but *Cai et al.* (2010) showed the area to have a very limited capacity for atmospheric CO_2 uptake. This low uptake capacity is thought to be the result of low biological productivity, surface warming, and a shallow mixed layer that can quickly equilibrate with the atmosphere. Based on their observations, *Cai et al.* (2010) concluded that the additional CO_2 uptake afforded by continued loss of sea ice in the Canada Basin is probably minimal.

This compelling hypothesis should motivate further examination of other Arctic regions. In this paper, we work towards that end by examining the CO_2 uptake capacity of the southeastern Canada Basin, adjacent to the Beaufort Sea (Figure 1). Previously, this region had retained relatively more sea ice in summer than the southwestern Canada Basin due to the southerly advection of ice within the Beaufort Gyre (*Hutchings and Rigor,* 2012). However, in

2012 a dramatic northwards retreat of the ice edge occurred (*NSIDC Arctic Sea Ice News and Analysis*, Sep. 19, 2012, http://nsidc.org/arcticseaicenews/), exposing surface waters in the region for an extended period of time. In light of this development, the objectives of this study are to assess the CO_2 uptake potential in this region of recent ice loss, and to compare our results with those obtained by *Cai et al.*, (2010) in order to paint a more complete picture of the potential atmospheric CO_2 uptake capacity of the Canada Basin.

2. Methods

From 27 August to 12 September, 2009, a multidisciplinary cruise was conducted in the southeastern Canada Basin onboard the CCGS *Amundsen*, as a joint International Polar Year effort between ArcticNet and GEOTRACES. The ship traveled north from the Mackenzie River delta (69.5^0N) along ~139^0W, eventually reaching 75.3^0N before returning along ~136^0W (Figure 1), stopping at several locations along the route to conduct sampling using a CTD/rosette system.

An underway pCO_2 system (General Oceanics model 8050) was operated throughout the cruise, sampling water from a high-volume inlet located near the bow of the ship at a nominal depth of 5 m. The system calibration was monitored with twice-daily checks against three certified gas standards (CO_2 concentrations of 0.0, 359.6, and 455.7 ppm). Although the system was located close to the inlet, a temperature gauge in the equilibrator recorded an increase of 1.0 ± 0.7^0C relative to on-station measurements made by the ship's CTD. This mean on-station offset was used to correct all pCO_2 measurements for thermodynamic effects, eliminating the warming bias but introducing an uncertainty of ±3% to the pCO_2 measurements. The underway system also housed a flow-through CTD (Idronaut model Ocean Seven 315) which provided

69 continuous salinity measurements.

70 At four of the stations visited on the cruise track (L1, L1.1, L2, L3, see Figure 1) a suite
71 of biogeochemical measurements were conducted on seawater samples collected by 12 L Niskin
72 bottles fixed on the rosette. To characterize the carbonate system, total alkalinity (TA) was
73 measured by open-cell potentiometric titration (Radiometer Analytical® TIM865 TitraLab) and
74 pH was measured by a UV-VIS diode-array spectrophotometer (Agilent-HP® 8453) using
75 phenol red and *m*-cresol purple indicators (*Mucci et al.,* 2010). The pH samples were handled
76 carefully to avoid equilibration with the atmosphere, and DIC and pCO_{2sw} values derived from
77 these measurements have been shown to be consistent with direct measurements (*Lansard et al.,*
78 2012; *Mucci et al.,* 2010). Hence, we calculated dissolved inorganic carbon (DIC) and pCO_2
79 from TA/pH measurements using CO2SYS (*Lewis and Wallace,* 1998) and the carbonic acid
80 dissociation constants of *Mehrbach et al.* (1973) as refit by *Dickson and Millero* (1987).
81 Concentrations of macronutrients (nitrate + nitrite, nitrite, phosphate, ammonium, and silicate)
82 were determined on fresh samples using standard colorimetric methods and an Autoanalyzer 3
83 (see *Tremblay et al.* (2008) for details). Seawater samples were also taken for stable oxygen
84 isotope analysis ($\delta^{18}O$), conducted at the Stable Isotope Geochemistry Laboratory (GEOTOP).
85 The $\delta^{18}O$ data were used in an optimum multiparameter (OMP) algorithm that also utilized
86 salinity and TA to quantify the fractional contributions of source water types to the surface water
87 mass at the sample sites. A description of the OMP and its full results will be published in a
88 forthcoming paper, but the relevant methodology, including the water type end-members and
89 their characteristics, is available in *Lansard et al.* (2012). For all CTD casts (including on-
90 station casts where biogeochemical sampling was not conducted), surface mixed layer depth was
91 calculated as the depth where potential density increased by 0.1 kg m^{-3} relative to the shallowest

92 measurement (*Toole et al.*, 2010).

93

94 **3. Observations**

95 In late summer 2009, the shelf seas in our study area were completely exposed to the
96 atmosphere (Figure 1), while the deep basin was covered by a heterogeneous sea ice cover that
97 extended to 150^{0}W (*Barber et al.*, 2009). As discussed in *Barber et al.* (2009) and *Galley et al.*
98 (in press), ice in the area between ~140^{0}W and ~135^{0}W was mostly heavily decayed first-year
99 sea ice interspersed with multi-year floes, and the mean thickness observed on helicopter surveys
100 ranged from 0.5 to 1.1 m. To the east of 135^{0}W was a tongue of multi-year ice that was much
101 thicker (mean ~1.8m), but still heavily decayed (Figure 1).

102 As Figure 1a shows, pCO_{2sw} under both of these ice types was considerably lower (mean
103 and standard deviation: 305 ± 10 μatm) than on the exposed shelf, where pCO_{2sw} ranged from
104 300-370 μatm. Spatial variability under the ice cover was muted, although pCO_{2sw} was slightly
105 higher (311 ± 5 μatm) on the western transect than on the eastern transect (301 ± 9 μatm), and
106 was lowest under the multi-year ice (289 ± 5 μatm). Lower salinity (mean 25.3 vs. 26.2, Figure
107 1b) and higher SST (mean -1.0^{0}C vs. -1.3^{0}C, Figure 1c) were observed on the west side of the
108 study area, and the highest salinities (mean 28.2) were observed under the multi-year ice.

109 A summary of the conditions observed at each station is shown in Table 1. The OMP
110 analysis reveals that much of the variability in the water properties (salinity, SST and chemical
111 composition) between stations can be explained by varying contributions of sea ice melt. At
112 stations L1 and L1.1, sea ice melt water composed 16-17% of the mass of the under-ice water,
113 while only accounting for 11% of the mass at stations L2 and L3. This influence of ice melt was
114 reflected in lower salinity, lower DIC and TA, and higher SST at the southern stations (Table 1),

and is probably also responsible for much of the heterogeneity apparent in the underway system data (Figure 1).

From the vertical profile data (see supplemental Figure S1), we generally observed a shallow mixed layer at the stations (mean depth 15.3 m with a range of 10 to 23 m), delimited by a sharp pycnocline. DIC, TA and pCO_2 increased rapidly with depth below the mixed layer (while pH decreased), whereas pCO_2 reached a maximum around 150 m depth (in the upper-halocline layer, e.g. *Lansard et al.*, (2012)). Macronutrient concentrations also peaked in that layer, but more relevant to the present study was a complete absence of nitrate, with small residuals of phosphate, silicate, and ammonium in the mixed layer (see also Table 1). Data from a fluorometer attached to the CTD showed a sub-surface chlorophyll maximum centered around 60 m, well below the mixed layer.

4. CO_2 Uptake Potential

To investigate atmospheric CO_2 uptake potential at each of the sampling stations, we performed a simple modeling exercise. At each station, the model calculates an initial surface DIC, TA, and pCO_2 assuming that the remaining ice cover melts completely (ice thicknesses for each station are shown in Table 1, and we use a sea ice melt end-member whose properties are: DIC= 330 μmol kg^{-1}, TA= 415 μmol kg^{-1}, salinity = 4.7 – average values from *Rysgaard et al.* (2009) and *Miller et al.* (2012), as reported by *Lansard et al.* (2012)). Since fixed inorganic nitrogen was depleted in the surface mixed layer, we assume that further biological pCO_2 reduction would be negligible. The model is then run at 6-hour intervals over a simulated 100-day open water season, assuming that the sea surface warms at a rate of 0.13 $^0C\ d^{-1}$ for 50 days and then cools at the inverse rate. This warming rate produces a maximum SST of 5^0C, which is

138 similar to satellite observations in the area during the 2012 ice retreat event (*NSIDC Arctic Sea*
139 *Ice News and Analysis,* Sep. 5, 2012, http://nsidc.org/arcticseaicenews/). At each 6-hour
140 interval, air-sea gas exchange is calculated as the product of the air-sea pCO_2 gradient (using 387
141 μatm as the atmospheric value), the gas transfer velocity (a function of wind speed, which we set
142 at a mean value 4.6 m s^{-1} based on measurements at nearby land-based weather stations) and the
143 gas solubility (a function of salinity and SST). Gas transfer velocity is calculated using the
144 quadratic expression appropriate for long-term mean winds described by *Wanninkhof et al.*,
145 (2002). At each time-step of the model, the mixed layer DIC and pCO_2 arising from gas
146 exchange is computed using a Matlab version of CO2SYS, and the results are passed on to the
147 next iteration of the model.
148 We also performed several sensitivity tests of the model, using the mean surface
149 conditions (and the above warming rate and wind velocity) for all stations as a baseline, and then
150 perturbing parameters that either had high uncertainty or were expected to have a strong
151 influence on the calculated CO_2 flux. For these tests the warming/cooling rate was varied
152 between 0.09 and 0.17 ^{0}C d^{-1} (the upper rate reflecting observations of *Else et al.*, (2012a) in
153 nearby Amundsen Gulf in 2008, the lower rate reflecting observations of *Cai et al.* (2010)),
154 surface mixed layer depth was varied between 10 and 23 m (reflecting the range of mixed layer
155 depths that we encountered during this study), wind velocity was varied between 4.0 and 5.2 m s^-
156 ^{1} (reflecting variability around the mean wind velocity observed at nearby weather stations) and
157 the TA:DIC ratio in sea ice melt water was varied between 1.1 and 1.5 (reflecting observed
158 variability in ice melt chemistry, e.g. *Rysgaard et al.* (2009)).
159 Results of the modeling exercise (Figure 2) support the hypothesis that the surface waters
160 in our study region cannot absorb significant amounts of atmospheric CO_2 during an extended

ice-free event. At the four stations, the mean CO_2 exchange rate over the 100-day model run ranged between -2.3 and -2.6 mmol m^{-2} d^{-1}, with an overall mean of -2.4 mmol m^{-2} d^{-1}. This mean value is ~60% lower than the mean uptake rate estimated by *Cai et al*. (2010) over a similar 100-day period in the southwestern Canada Basin.

Perhaps the most interesting feature of our model results is the "overshoot" that occurs after less than one month, when sea surface warming causes pCO_{2sw} to exceed the atmospheric value by about 30 µatm (Figure 2a). We observed a similar phenomenon in Amundsen Gulf in 2008 (*Else et al.*, 2012a), although the degree of oversaturation was not as significant (~10 µatm). The modeled oversaturation occurs over a period of about 27 days (Figure 2b), limiting the total amount of CO_2 that the surface waters can absorb. Consequently, little DIC is actually added to the surface water over the 100-day period; for the four stations that we modeled, DIC only increased by an average of 18 µmol kg^{-1} by the end of the model run. This phenomenon occurs because some of the DIC added during the initial uptake period is subsequently released during the outgassing period. The uptake period that follows as the surface water cools towards its freezing point is then insufficient to allow pCO_2 to reach equilibrium, and the result is undersaturation at the end of the open water season – a condition observed across much of the Beaufort Shelf in 2008 (*Else et al.*, 2012).

In their analysis, *Cai et al.* (2010) emphasized the rapid equilibration of the shallow surface mixed layer as a critical factor inhibiting significant uptake of atmospheric CO_2. Our results highlight that the rapid warming that occurs in this layer when the ice is removed is another critical component of the system. The sensitivity tests show that over the range of conditions expected for our study area (Figure 2c), the potential for atmospheric CO_2 uptake is most sensitive to surface warming. Furthermore, generating a pCO_2 oversaturation requires a

184 relatively small increase in SST; modeled pCO_{2sw} at all stations exceeded the atmospheric value
185 when SST reached approximately 3°C. Overall, our sensitivity analysis confirmed that weak
186 uptake is expected in this area following sea ice retreat no matter how the model is perturbed,
187 and that this section of the Canada Basin has a lower potential for absorbing atmospheric CO_2
188 than the area examined by *Cai et al.*, (2010).
189
190 **5. Discussion**
191 Why then do surface waters in the southeastern Canada Basin have a smaller potential to
192 absorb atmospheric CO_2 than in the southwestern Canada Basin? To address this question it is
193 important to understand that although connected by the Beaufort Gyre, the surface waters in the
194 two regions have slightly different compositions arising from variations in shelf-basin, air-sea,
195 and sea-ice interactions (*Macdonald et al.*, 2002). Most notably, the basin waters that *Cai et*
196 *al.* (2010) studied are influenced by outflow from the highly productive Chukchi Shelf. Chukchi
197 Shelf water is characterized by a high TA:DIC ratio and therefore a strong capacity to absorb
198 atmospheric CO_2, as reflected in observations of Revelle Factors (RF) in the range of 6-8 (*Bates*
199 *et al.*, 2006). In the past, this strong buffering capacity prevented waters on the Chukchi Shelf
200 from absorbing enough DIC from the atmosphere to reach equilibrium before being exported to
201 the deep basin (*Anderson et al.*, 2010). The outflow from the Chukchi Shelf was thus thought to
202 provide the deep basin with a continuous supply of water with significant potential to absorb
203 atmospheric CO_2. Of course, the results of *Cai et al.* (2010) suggest that longer open water
204 seasons may be eroding that potential. Meanwhile, shelf waters in our study area have relatively
205 high RF values; *Shadwick et al.* (2011) found RF values around 14 in spring and as high as 19
206 through the winter in the southeastern Beaufort Sea. The source water type analysis (Table 1)

shows that shelf water did not make up a significant fraction of surface mixed layer in this area in 2009, but even in years where shelf-basin exchange is more important (e.g. *Macdonald et al.* (2002)) our study area does not stand to gain any significant uptake capacity from shelf waters.

In addition to regional variations, it is possible that our results reflect the ongoing evolution of decreased CO_2 uptake capacity in the Canada Basin, as predicted by *Cai et al.* (2010). In the past, DIC-undersaturated surface water that exited the Chukchi Shelf was precluded from further air-sea gas exchange by the perennial sea ice cover that existed in the Canada Basin (*Anderson et al.*, 2010). Under this scenario, the surface water in our area (which is linked through the Beaufort Gyre) would be expected to retain some of that initial CO_2 uptake potential. However, open-water seasons were particularly long in 2007 and 2008 (e.g. 25-100 days longer in 2007 than 2006, as per *Arrigo et al.* (2008)) across much of the Chukchi Sea and Canada Basin. Since *Cai et al.*, (2010) showed that CO_2 uptake potential can essentially be eliminated by a 100-day open water season, what we may be seeing in our results is the cumulative erosion of uptake capacity in the Canada Basin associated sea ice extent reductions in recent years.

How this situation evolves in the Canada Basin in the future is of course uncertain. Longer open water seasons will alleviate light limitation on primary production (*Arrigo et al.*, 2008), potentially enhancing biological reduction of pCO_{2sw}. However, the nutrient limitation that seems to be ubiquitous across the Canada Basin (Figure S1, *Cai et al.*, (2010); *Jutterström and Anderson* (2010)) will significantly constrain this effect. In the future, nutrients may be replenished by enhanced upwelling permitted by more extensive open water (e.g. *Tremblay et al.*, 2011), but strong upwelling may episodically bring the carbon-rich upper-halocline layer into contact with the atmosphere – a phenomenon which can transition weak CO_2 sink areas into CO_2

sources (*Else et al.*, 2012a, 2012b; *Lansard et al.* 2012, *Mathis et al.*, 2012; *Mucci et al.*, 2010). Conversely, changing sea ice processes have the potential to push the system towards stronger uptake; the sea ice pump (which describes the partitioning of DIC-enriched brine at depth and TA-enriched melt water at the surface, e.g. *Rysgaard et al.*, (2009)) may become more effective with a transition from perennial to annual sea ice, and uptake during initial ice formation (*Anderson et al.*, 2004; *Else et al.*, 2011) may become more widespread as the area undergoing freeze-thaw cycles expands. Finally, a significant freshening of the Canada Basin has been observed in the last decade (*McPhee et al.*, 2009; *Morrison et al.*, 2012; *Yamamoto-Kawai et al.*, 2009), increasing surface stratification and modifying carbonate chemistry (*Yamamoto-Kawai et al.*, (2009)). Ultimately, the net effect of these climate change impacts on CO_2 uptake in the future remains to be seen, but for now all evidence points to very limited atmospheric CO_2 uptake as the waters of the Canada Basin become increasingly exposed to the atmosphere.

Acknowledgements

Authors of this paper are members of ArcticNet (funded in part by NCE, NSERC, CIHR and SSHRC) and the Arctic Science Partnership. Additional support was provided through the Canada Excellence Research Chair in Arctic Geomicrobiology and Climate Change, and from the Centre for Earth Observation Science at the University of Manitoba. Many thanks are owed to the captains, crew, and research technicians onboard the CCGS *Amundsen*.

References

AMAP, 2011. Snow, Water, Ice and Permafrost in the Arctic (SWIPA): Climate Change and the Cryosphere. Arctic Monitoring and Assessment Programme (AMAP), Oslo, Norway.

Anderson, L. G., E. Falck, E. P. Jones, S. Jutterström, and J. H. Swift (2004), Enhanced uptake of atmospheric CO_2 during freezing of seawater: A field study in Storfjorden, Svalbard, *J. Geophys. Res.*, *109*, C06004, doi:10.1029/2003JC002120.

Anderson, L. G., T. Tanhua, G. Björk, S. Hjalmarsson, E.P. Jones, S. Jutterström, B. Rudels, J.H. Swift, and I. Wåhlström (2010), Arctic ocean shelf-basin interaction: An active continental shelf CO_2 pump and its impact on the degree of calcium carbonate solubility. *Deep-Sea Res. I*, 57:869-879, doi:10.1016/j.dsr.2010.03.012

Arrigo, K. R., G. van Dijken, and S. Pabi (2008), Impact of a shrinking Arctic ice cover on marine primary production, *Geophys. Res. Lett.*, *35*, L19603, doi:10.1029/2008GL035028.

Barber, D.G., R. Galley, M.G. Asplin, R. De Abreu, K.-A. Warner, M. Pućko, M. Gupta, S. Prinsenberg, and S. Julien (2009), Perennial pack ice in the Beaufort Sea was not as it appeared in the summer of 2009. *Geophys. Res. Lett.*, 36:L24501, doi:10.1029/2009GL041434.

Bates, N. R., S. B. Moran, D. A. Hansell, and J. T. Mathis (2006), An increasing CO_2 sink in the Arctic Ocean due to sea-ice loss, *Geophys. Res. Lett.*, *33*, L23609, doi:10.1029/2006GL027028.

Bates, N. R. and J.T. Mathis (2009), The Arctic Ocean marine carbon cycle: evaluation of air-sea CO_2 exchanges, ocean acidification impacts and potential feedbacks. *Biogeosciences*, 6(11):2433–2459 , doi:10.5194/bg–6–2433–2009.

Cai, W., et al. (2010), Decrease in the CO_2 uptake capacity in an ice-free Arctic Ocean basin. *Science*, 329(5991):556–559, doi:10.1126/science.1189338

Dickson, A.G. and F. J. Millero (1987), A comparison of the equilibrium constants for the dissociation of carbonic acid in seawater media. *Deep-Sea Res.* **34**, 1733-1743.

Else, B. G. T., T. N. Papakyriakou, R. J. Galley, W. M. Drennan, L. A. Miller, and H. Thomas (2011), Wintertime CO_2 fluxes in an Arctic polynya using eddy covariance: Evidence for enhanced air-sea gas transfer during ice formation, *J. Geophys. Res.*, *116*, C00G03, doi:10.1029/2010JC006760.

Else, B. G. T., T.N. Papakyriakou, R.J. Galley, A. Mucci, M. Gosselin, L.A. Miller, E.H. Shadwick, and H. Thomas (2012a), Annual cycles of pCO_{2sw} in the southeastern Beaufort Sea: New understandings of air–sea CO_2 exchange in Arctic polynya regions. *J. Geophys. Res.*, 117:C00G13, doi:10.1029/2011JC007346

Else, B. G. T., R. J. Galley, T. N. Papakyriakou, L. A. Miller, A. Mucci, and D. Barber (2012b), Sea surface pCO_2 cycles and CO_2 fluxes at landfast sea ice edges in Amundsen Gulf, Canada, *J. Geophys. Res.*, *117*, C09010, doi:10.1029/2012JC007901.

Galley, R.J., B.G.T. Else, S.J. Prinsenberg, and D.G. Barber (in press), Sea ice concentration, extent, age, motion and thickness in regions of proposed offshore oil and gas development near the Mackenzie Delta - Canadian Beaufort Sea. *Arctic*, MS# 11-175.

Hutchings, J. K., and I.G. Rigor (2012), Role of ice dynamics in anomalous ice conditions in the Beaufort Sea during 2006 and 2007, *J. Geophys. Res.*, 117, C00E04, doi:10.1029/2011JC007182.

Jutterström, S. and L.G. Anderson (2010), Uptake of CO_2 by the Arctic Ocean in a changing climate. *Mar. Chem.*, 122, 96-104, doi: 10.1016/j.marchem.2010.07.002.

298 Lansard, B., A. Mucci, L.A. Miller, R.W. MacDonald, and Y. Gratton (2012), Seasonal
299 variability of water mass distribution in the southeastern Beaufort Sea determined by total
300 alkalinity and $\delta^{18}O$. *J. Geophys. Res.*, 117:C03033, doi:10.1029/2011JC007299.
301 Lewis, E. and D.W.R. Wallace (1998), Program developed for CO2 system calculations, *Rep.*
302 *ORNL/CDIAC-105*, Carbon Dioxide Inf. Anal. Cent., Oak Ridge Natl. Lab., U.S. Dep. Of
303 Energy, Oak Ridge, Tenn. [Available at http://cdiac.esd.ornl.gov/oceans/co2rprt.html.]
304 Macdonald, R.W., F.A. McLaughlin, and E.C. Carmack (2002), Fresh water and its sources
305 during the SHEBA drift in the Canada Basin of the Arctic Ocean. *Deep-Sea Res. I*,
306 49:1769-1785, doi:10.1029/JC094iC12p18057
307 Mathis, J. T., et al. (2012), Storm-induced upwelling of high pCO_2 waters onto the continental
308 shelf of the western Arctic Ocean and implications for carbonate mineral saturation
309 states, *Geophys. Res. Lett.*, *39*, L07606, doi:10.1029/2012GL051574.
310 McPhee, M. G., A. Proshutinsky, J. H. Morison, M. Steele, and M. B. Alkire (2009), Rapid
311 change in freshwater content of the Arctic Ocean, *Geophys. Res. Lett.*, *36*, L10602,
312 doi:10.1029/2009GL037525.
313 Mehrbach, C., C. H. Culberson, J. E. Hawley, and R. N. Pytkowicz. (1973), Measurement of the
314 apparent dissociation constants of carbonic acid in seawater at atmospheric pressure.
315 *Limnol. Oceaogr.* 18(6), 897-907.
316 Miller, L. A., T. N. Papakyriakou, R. E. Collins, J. W. Deming, J. K. Ehn, R. W. Macdonald, A.
317 Mucci, O. Owens, M. Raudsepp, and N. Sutherland (2011), Carbon dynamics in sea ice:
318 A winter flux time series, *J. Geophys. Res.*, *116*, C02028, doi:10.1029/2009JC006058.
319 Morison, J., R. Kowk, C. Peralta-Ferriz, M. Alkire, I. Rigor, R. Anderson and M. Steele (2012),
320 Changing Arctic Ocean freshwater pathways, *Nature*, 481, doi:10.1038/nature10705

321 Mucci, A., B. Lansard, L. A. Miller, and T. N. Papakyriakou (2010), CO_2 fluxes across the air-
322 sea interface in the southeastern Beaufort Sea: Ice-free period, *J. Geophys. Res., 115*,
323 C04003, doi:10.1029/2009JC005330.
324 Rysgaard, S., J. Bendtsen, L.T. Pedersen, H. Ramløv, and R.N. Glud (2009), Increased CO_2
325 uptake due to sea ice growth and decay in the Nordic Seas. *J. Geophys. Res.*,
326 114:C09011, doi:10.1029/2008JC005088
327 Shadwick, E. H., et al. (2011), Seasonal variability of the inorganic carbon system in the
328 Amundsen Gulf region of the southeastern Beaufort Sea. *Limnol. Oceaogr.*, 56(1), 303-
329 322, doi: 10.4319/lo.2011.56.1.0303
330 Toole, J.M., M.-L. Timmermans, D.K. Perovich, R.A. Krishfield, A. Proshutinsky, and J.A.
331 Richter-Menge (2010), Influences of the ocean surface mixed layer and thermohaline
332 stratification on Arctic Sea ice in the central Canada Basin. *J. Geophys. Res.*, 115,
333 C10018, doi:10.1029/2009JC005660.
334 Tremblay, J.-É., K. Simpson, J. Martin, L. Miller, Y. Gratton, D. Barber, and N.M. Price (2008),
335 Vertical stability and the annual dynamics of nutrients and chlorophyll fluorescence in
336 the coastal, southeast Beaufort Sea. *J. Geophys. Res.*, 113:C07S90,
337 doi:10.1029/2007JC004547.
338 Tremblay, J.-É., et al. (2011), Climate forcing multiplies biological productivity in the coastal
339 Arctic Ocean, *Geophys. Res. Lett.*, 38, L18604, doi:10.1029/2011GL048825.
340 Wanninkhof, R., Doney, S.C., Takahashi, T., and W.R. McGillis (2002), The effect of using
341 time-averaged winds on regional air-sea CO_2 fluxes. In, *Gas Transfer at Water Surfaces*,
342 AGU, Washington, DC, *Geophysical Monograph* 127, 351-356.
343 Yamamoto- Kawai, M., F. A. McLaughlin, E. C. Carmack, S. Nishino, K. Shimada, and N.
344 Kurita (2009a), Surface freshening of the Canada Basin, 2003–2007: River runoff versus

sea ice meltwater, *J. Geophys. Res.*, *114*, C00A05, doi:10.1029/2008JC005000.

Yamamoto- Kawai, M., F. A. McLaughlin, E. C. Carmack, S. Nishino, and K. Shimada (2009b), Aragonite undersaturation in the Arctic Ocean: Effects of ocean acidification and sea ice melt, *Science*, 326(5956), doi:10.1126/science.1174190

Figure 1. Underway surface water measurements: (a) observed pCO_2, (b) salinity, and (c) sea surface temperature, overlain on a composite of RADARSAT-1 images collected during the study period. The sampling stations (including a multi-year ice sampling station labeled "MYI") are indicated. The black line indicates the approximate location of the multi-year ice tongue based on Canadian Ice Service charts, and the dashed line delineates the location of lower concentration ice composed of a mixture of first-year and multi-year floes.

Figure 2. Results from the air-sea gas exchange model: (a) pCO_{2sw} evolution during the model runs for the four sampling stations, with the horizontal line denoting atmospheric pCO_2; (b) air-sea CO_2 flux evolution during the model runs for the four sampling station, with mean CO_2 flux for the 100-day period noted for each station as $\overline{F_{CO_2}}$; (c) air-sea CO_2 flux evolution during the sensitivity runs, with $\overline{F_{CO_2}}$ noted for each run.

Table 1. Summary of surface water conditions (3-4m depth) observed at the four sampling stations. The results of the optimum multiparameter analysis are also shown as the mass percentage of each water type (MW = Mackenzie River water, SIM = Sea ice melt water, PML = polar mixed layer water) that makes up the surface water at the four stations. Ice thicknesses are from *Galley et al.* (in press), and ice concentrations are from Canadian Ice Service charts.

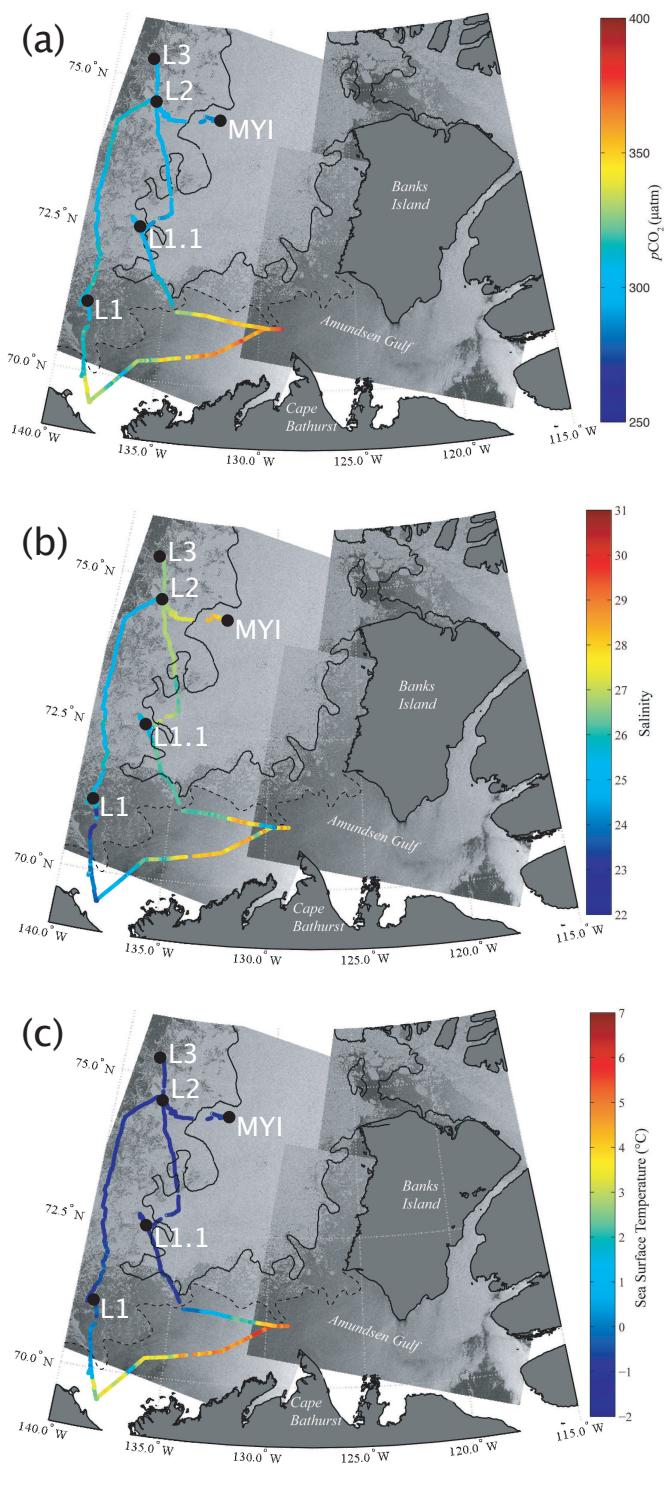
(a)
L3
L2
MYI
L1.1
L1
Banks Island
Amundsen Gulf
Cape Bathurst
75.0°N
72.5°N
70.0°N
140.0°W
135.0°W
130.0°W
125.0°W
120.0°W
115.0°W
400
350
300
250
pCO2 (µatm)
(b)
L3
L2
MYI
L1.1
L1
Banks Island
Amundsen Gulf
Cape Bathurst
75.0°N
72.5°N
70.0°N
140.0°W
135.0°W
130.0°W
125.0°W
120.0°W
115.0°W
31
30
29
28
27
26
25
24
23
22
Salinity
(c)
L3
L2
MYI
L1.1
L1
Banks Island
Amundsen Gulf
Cape Bathurst
75.0°N
72.5°N
70.0°N
140.0°W
135.0°W
130.0°W
125.0°W
120.0°W
115.0°W
7
6
5
4
3
2
1
0
−1
−2
Sea Surface Temperature (°C)

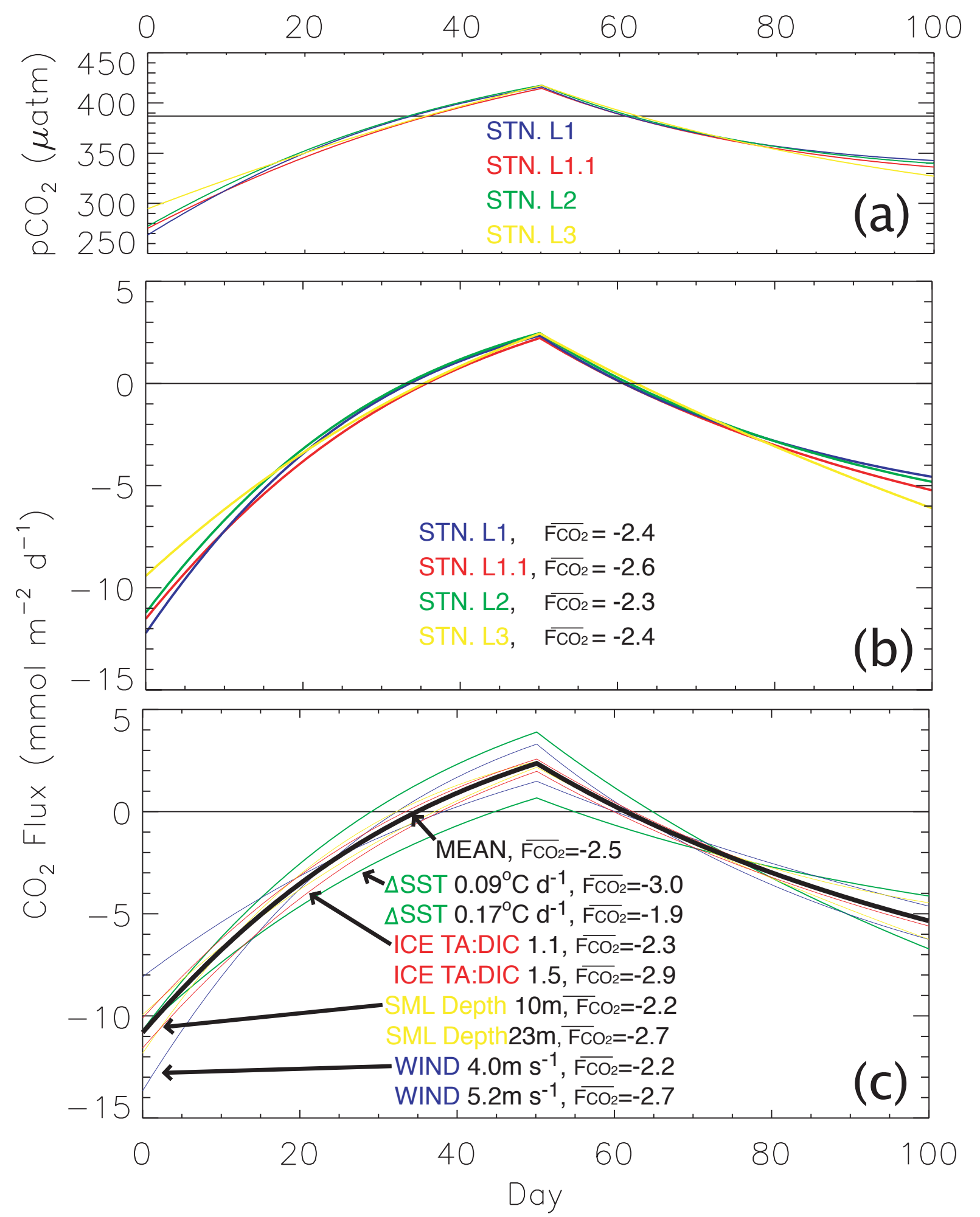
0
20
40
60
80
100
pCO2 (μatm)
450
400
350
300
250
STN. L1
STN. L1.1
STN. L2
STN. L3
(a)
5
0
−5
−10
−15
CO2 Flux (mmol m−2 d−1)
STN. L1, FCO2 = -2.4
STN. L1.1, FCO2 = -2.6
STN. L2, FCO2 = -2.3
STN. L3, FCO2 = -2.4
(b)
MEAN, FCO2=-2.5
ΔSST 0.09°C d-1, FCO2=-3.0
ΔSST 0.17°C d-1, FCO2=-1.9
ICE TA:DIC 1.1, FCO2=-2.3
ICE TA:DIC 1.5, FCO2=-2.9
SML Depth 10m, FCO2=-2.2
SML Depth23m, FCO2=-2.7
WIND 4.0m s-1, FCO2=-2.2
WIND 5.2m s-1, FCO2=-2.7
(c)
Day

Station	L1	L1.1	L2	L3
Date	31-Aug	9-Sep	4-Sep	7-Sep
Depth (m)	1914	2533	3000	3000
SST (^{0}C)	-1.039	-1.34	-1.401	-1.388
Salinity	25.536	25.267	26.736	26.454
pH	8.0562	8.0804	8.0966	8.0906
TA (µmol L^{-1})	1842.3	1850.0	1951.9	1944.7
DIC (µmol L^{-1})	1772.3	1777.0	1867.0	1862.0
Revelle Factor	17.9	17.8	17.2	17.3
pCO_2 (µatm)*	316	301	305	301
pCO_2 (µatm)**	309	300	304	300
Nitrate (µmol L^{-1})	not collected	0	0.15	0.06
Phosphate (µmol L^{-1})	not collected	2	1.5	2.3
Silicate (µmol L^{-1})	not collected	0.5	0.55	0.51
Ammonium (µmol L^{-1})	not collected	0.04	0.01	0.01
MW %	7	9	8	9
SIM %	17	16	11	12
PML %	75	75	81	80
Ice Thickness (m)	1.09	0.86	0.65	0.49
Ice Concentration (10^{ths})	6	8	9	9

*Calculated from TA/pH using CO2SYS

**From underway pCO2 system